



Failure Analysis of Low-Pressure Evaporator in Heat Recovery Steam Generator with 200 ton/h of Capacity

Tri Sigit Purwanto · Diki Ismail Permana · Meilinda Nurbanasari · Abdurrachim · Muhammad Pramuda Nugraha Sirodz

Submitted: 6 June 2023 / in revised form: 14 August 2023 / Accepted: 6 September 2023 / Published online: 27 October 2023
© The Author(s) 2023

Abstract A steam-gas power plant (SGPP) combines a gas power plant (GPP) and a steam power plant by using the exhaust gas from the GPP to produce steam in the heat steam recovery generator (HRSG). The SGPP, which has a 200 ton/h HRSG capacity, experienced cracks, ruptures, and fatigue at the connection of the low-pressure evaporator pipe. Fatigue is a common failure mechanism in mechanical components due to thermal stress. However, the exact cause of the failure was unknown; therefore, a root cause analysis was conducted. Analysis included the thickness, metallography, chemical composition, tensile testing, thermography, defect testing, and hardness testing. The research showed thermal stresses were the cause of the low-pressure evaporator HRSG pipe failure. In addition, inspection results revealed a decrease in tensile strength, material hardness, and thermal expansion that exceeded the allowed limit.

Keywords Failure analysis · HRSG · Thermal stress · Evaporator · Material pipe

Introduction

The heat recovery steam generator (HRSG) is a piece of equipment used in combined cycle power plant systems. Its function is to utilize the heat from the combustion gases that exit a gas turbine to produce the steam needed by the turbine. The SGPP system can operate independently with the GPP system and without the SPP system by closing the diverter damper flap to the HRSG. The HRSG system consists of a high-pressure (HP) superheater, an HP evaporator, an HP2 economizer, a low-pressure (LP) evaporator, an HP1 economizer, and an LP economizer. If the HRSG equipment is used continuously, its reliability value will decrease due to usage over time and various factors that may cause equipment failure [1, 2]. During the start-up process, the most critical factor is the rapid increase of all operating parameters, including temperature, pressure, and mass flow. During this period, the HRSG components, especially the steam drum, are subject to high thermal stress caused by uneven metal temperature distribution [3]. HRSG tube failure is one of the most frequent causes of forced power plant outages [4]. In a local power plant, one of the boilers has experienced several defects and failures after running for approximately 85,000 h [5]. HRSG failures often affect the performance of power generations system [2–6]. It has been reported that HRSG pipe failures are generally caused by creep damage [7–9], fatigue [10–12], excessive thermal stresses, water/steam corrosion [13], and short-term overheating [14].

The SGPP which is being studied in this paper has six HRSGs with a capacity of 200 ton/h each, and all face the same issue: failures in the LP evaporator, particularly in the west-side pipe (outlet pipe). This study focuses on one HRSG, examining its temperature and pressure

T. S. Purwanto · D. I. Permana (✉) · M. Nurbanasari · M. P. N. Sirodz
Mechanical Engineering Department, Faculty of Industrial Engineering, Institut Teknologi Nasional Bandung, Bandung, Indonesia
e-mail: permana.diki.ismail@phd.uni-mate.hu

D. I. Permana
Doctoral Study of Mechanical Engineering, Szent Istvan Campus, Hungarian University of Agriculture and Life Science, Godollo, Hungary

Abdurrachim
Department of Mechanical Engineering, Faculty of Engineering, University of Pasundan, Bandung, Indonesia

distribution, as shown in Fig. 1. The failure analysis of the HRSG system is centered on the LP evaporator, and a detailed schematic of the inlet and outlet section is depicted in Fig. 2 with a red circle. The LP evaporator's working pressure is three bar-G, with flue gas inlet and outlet temperatures of approximately 241.4 and 167.1 °C, respectively. The low-pressure system's resulting steam flow rate is 65.4 ton/h. A rupture in the low-pressure evaporator pipe can cause the entire system to cease functioning, so investigating the causes of the pipe's failure was imperative.

In Fig. 3, it is apparent that there was a leak in the LP evaporator pipe that had been in operation for over four years. The leak was located on the side of the pipe, while the connection with the header was leaking on the inner side of the pipe. This investigation aimed to determine the mechanism and cause of the low-pressure evaporator failure in HRSG pipes with a capacity of 200 ton/h at SGPP to prevent it from happening again in the future. Additionally, this study aimed to provide useful maintenance information and minimize unplanned downtime incidents.

Methodology

Leakage failure at the LP Evaporator HRSG was a recurrent issue in all HRSG units operated at the SGPP studied in this paper. Therefore, various experimental and measurement methods were necessary to determine the cause of failure. Some of these methods included visual investigation, ultrasonic thickness (UT) thickness, microstructural analysis, verification of material composition, hardness and tensile tests, and thermal analysis.

A visual examination was conducted on both the west-side and east-side pipes of the LP evaporator near the failure zone, and images were taken to document the nature of the failure. The visual inspection was performed using both the naked eye and a portable magnifying lens. Additionally, the exterior diameter of the failed tube was measured both at the point of failure and in an unbroken zone.

Moreover, non-destructive testing (NDT) was conducted to support the visual inspection, using section V of the American Society of Mechanical Engineering (ASME) Boiler and Pressure Vessel Code, and American Standard

Fig. 1 The HRSG schematic with temperature and pressure distributions

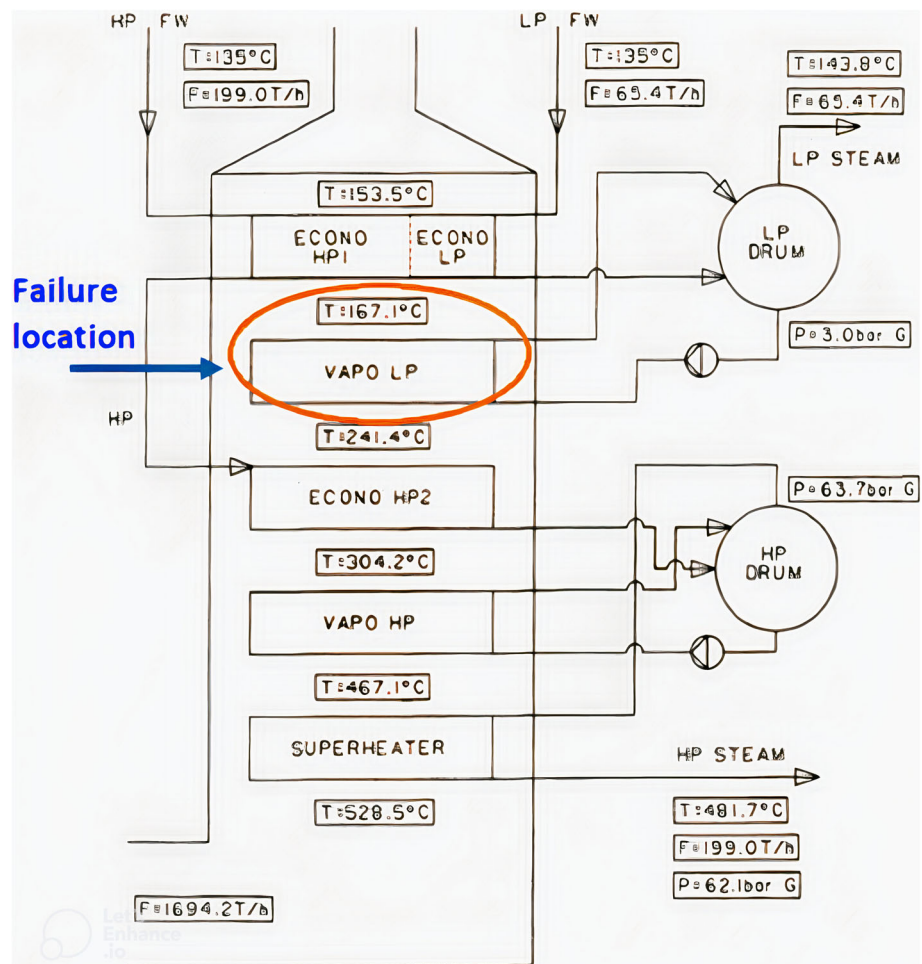


Fig. 3 Failure location: (a) leak on pipe and header joint and (b) leaks on the pipe bend

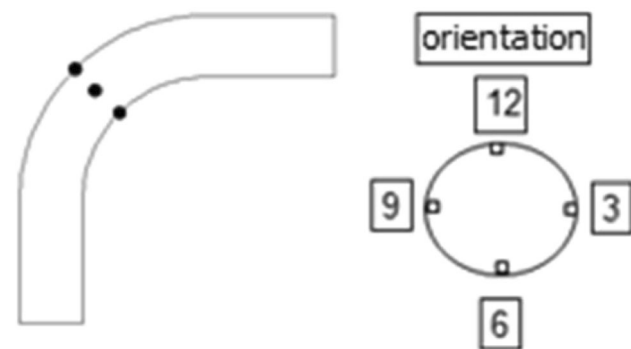
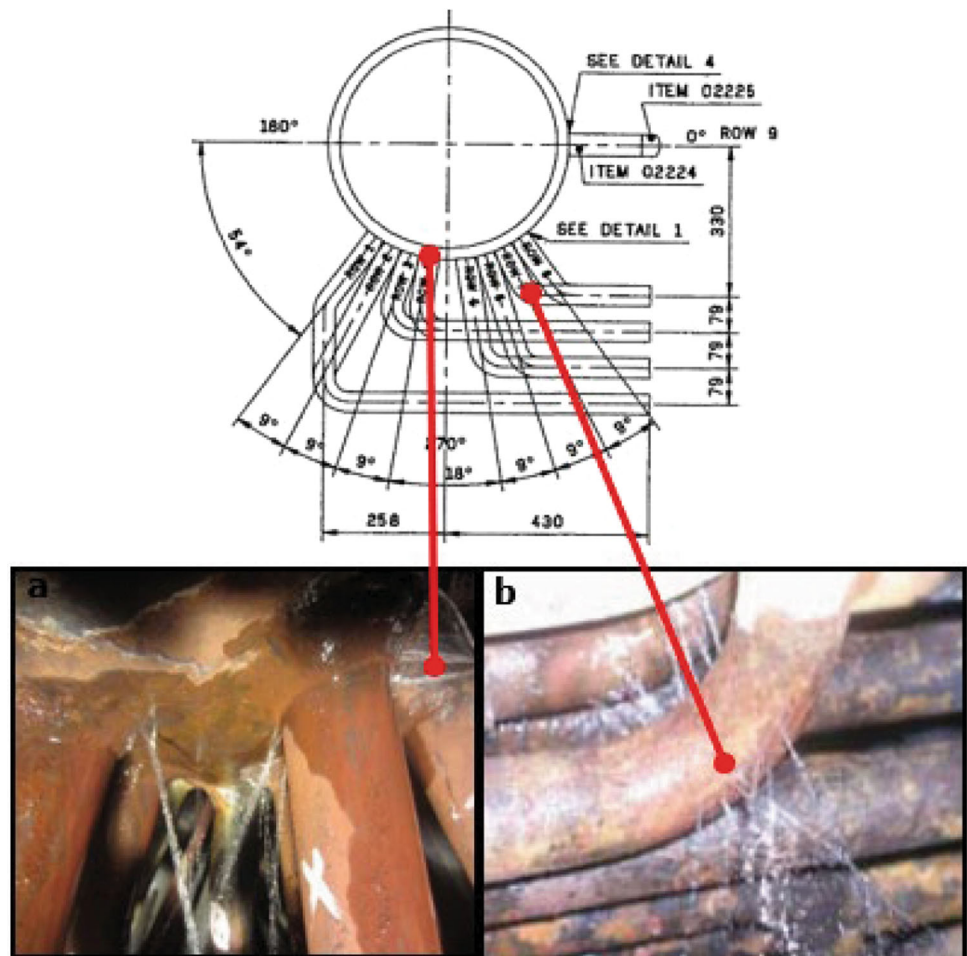


Fig. 4 Thickness measurement orientation

the difference is necessary. Additionally, hardness testing was conducted on samples taken from the failed pipes using the Brinell hardness (HB) measurement. In both the tensile and hardness tests, three samples were utilized from both the east and west sides of the LP evaporator pipes.

A simplified method was used to determine the flexibility of the LP evaporator pipe and whether it was at risk of thermal failure. This method assumed that the ambient temperature had been reached during the LP evaporator

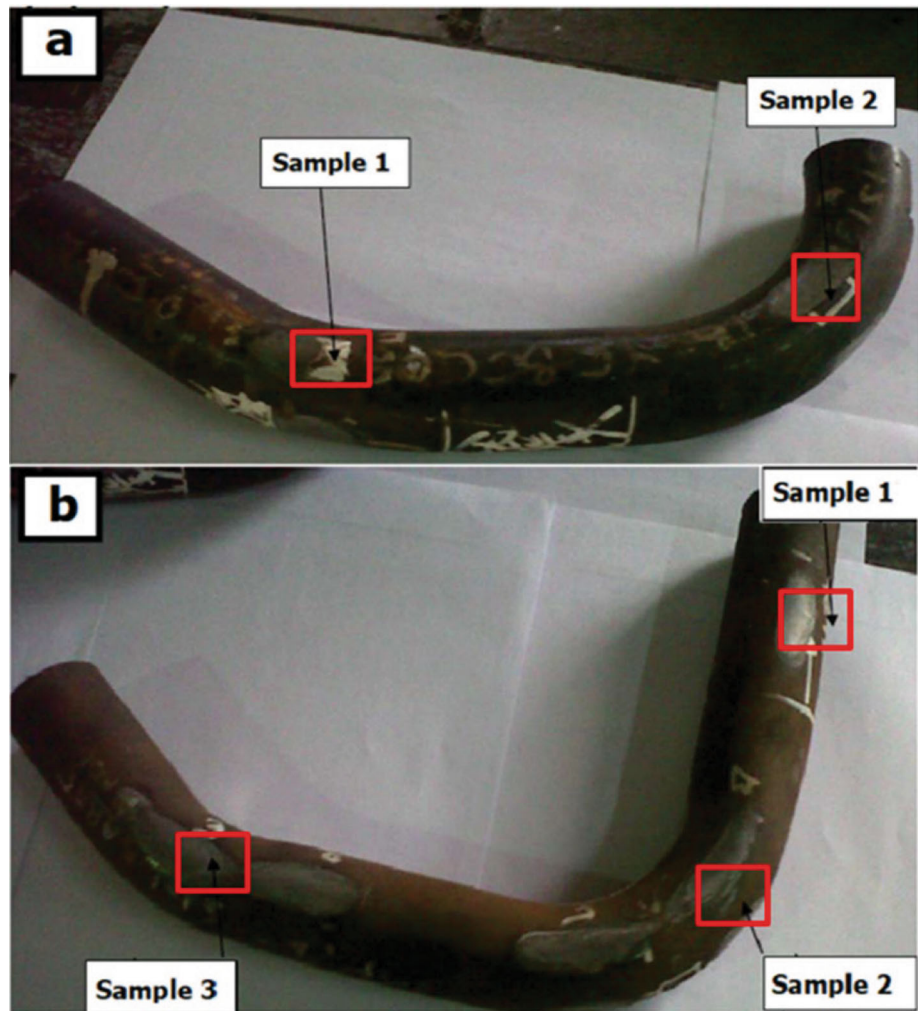
installation process. During operation, the LP evaporator pipe is filled with high-temperature steam, causing it to expand. This expansion leads to an increase in the length of the pipe while the distance between supports remains constant. Consequently, the pipe will bend and place a bending load on both the pipe and its supports. If the bending moment is significant enough, the stress placed on the material will exceed its strength, resulting in the failure of the LP evaporator.

In general, the formula for steel pipes is represented by Eq 1 as follows [15]:

$$\frac{(D \cdot Y)}{(L - U)^2} < 0.03 \tag{Eq 1}$$

where D denotes the pipe outer diameter (m), L denotes the total length of the LP evaporator pipe (m), and Y denotes the resultant of thermal growth to be absorbed (m), while U is the modulus constant of elasticity of material. The inequality suggests that the relative change in length due to thermal expansion should be less than 0.03, which might be a specified limit for a particular application to ensure that the expansion does not exceed a certain threshold.

Fig. 5 Specimen test sample: (a) east side pipe and (b) west-side pipe



The thermal diffusivity of the steel pipe is expressed in Eq 2 [15]:

$$\alpha = (11.56 + 0.0055T) \times 10^6 \quad (\text{Eq 2})$$

The subsequent procedure involves computing the resulting expansion of the pipe (y_r) in both horizontal (y_h) and vertical (y_v) directions, as illustrated by Eqs (3)–(5) [15].

$$y_v = (\alpha_1 T_1 l_v) - (\alpha_2 T_a l_v) \quad (\text{Eq 3})$$

$$y_h = (\alpha_1 T_1 l_h) - (\alpha_2 T_a l_h) \quad (\text{Eq 4})$$

$$y_R = \sqrt{y_v^2 + y_h^2} \quad (\text{Eq 5})$$

where T_1 denotes the inlet temperature, T_a denotes the ambient temperature of the pipe, and l_v and l_h denote the length of the pipe sections (m) in the vertical and horizontal directions, respectively. Table 1 presents the parameters of the LP evaporator pipes employed in the equations.

Table 1 The parameters of the LP evaporator pipes

Parameters	Value	Units
Length (L)	46.8	m
Tube diameter (D)	0.445	m
Header distance (U)	15.64	m
Ambient temperature (T_a)	27	°C
Inlet temperature (T_1)	280	°C
Outlet temperature (T_2)	90	°C

Temperature monitoring of the HRSG during the operation was conducted using a thermography device that displays the surface temperature of the object being observed. By color-coding the image captured, accurate surface temperature distribution can be determined. To monitor the temperature of the HRSG, recordings are specifically taken on the LP evaporator on both the east and west sides, precisely at the header pipe connections leading to the steam drum.

Analysis and Discussion

Visual Inspection and NDT

The investigation found cracks and leaks in the bends and joints between the evaporator pipe and the evaporator header of the steam outlet side (see Fig. 3a). The LP evaporator pipe material is ST37.8 CL1, with a diameter of 44.5 mm and a thickness of 2.9 mm. The evaporator header material is ST35.8, with a diameter of 508 mm and a thickness of 25 mm. The LP evaporator system uses 80 pipes with three passes. The repeated weld repair of the header and pipe joints in the east, as depicted in Fig. 3b, indicated that these failures have occurred frequently. The welding is necessary due to the pipe connection to the header, which frequently leaks, and as a result, the weld can increase the brittleness and induce cracks in the header.

Non-destructive testing (NDT) was conducted to enhance the visual inspection and identify the reason behind the LP evaporator pipe's failure. As shown in Fig. 6, NDT revealed a red area in the tube joint and the LP

evaporator pipe's outlet, suggesting a potential leak in that region. Additional findings presented in Fig. 7, indicated the same occurrence in the inlet side of the welded connection area between the header and pipes, with a red hue around the zone, indicating some sort of failure.

Ultrasonic Thickness Measurements

The ultrasonic thickness measurements focus on pipe bends since the outermost part of the bend is typically the thinnest and most critical. Thinning is often due to corrosion, as well as erosion caused by fluid colliding with the pipe wall. Thickness measurements were taken on the inlet and outlet sides of the LP evaporator pipe in both the west and east, with the results shown in Table 2. As seen in Table 2, the C3 section of the pipe had the smallest thickness at 2.15 mm compared to nominal design thickness of 2.9 mm. So there was 0.75 mm of wall thickness lost (approximately 26%) due to erosion. This measurement strongly suggested that erosion in the LP evaporator pipe is one of the major concern. As such, the minimum thickness

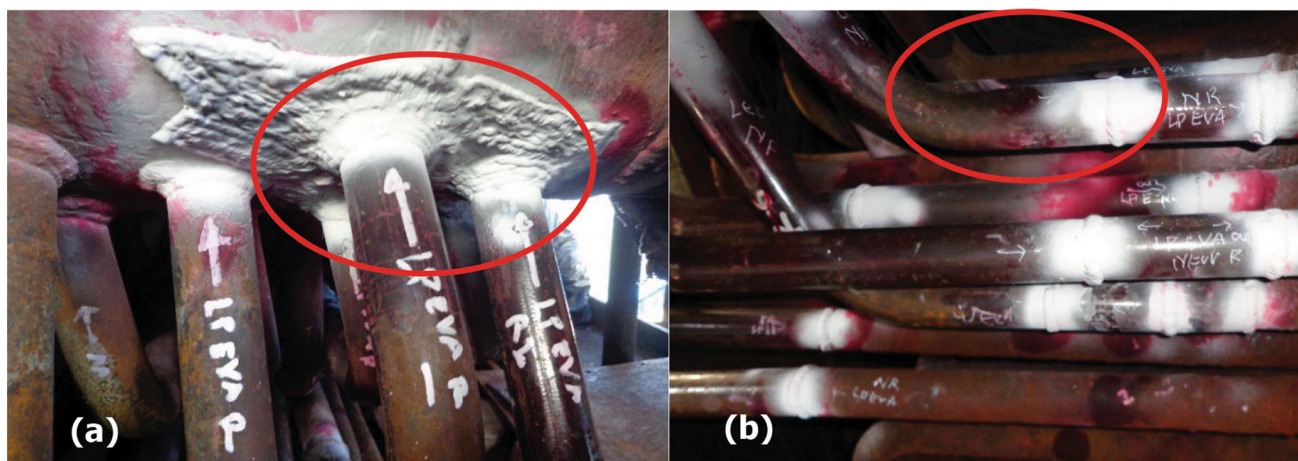


Fig. 6 NDT of the LP evaporator outlet: (a) header and (b) pipes

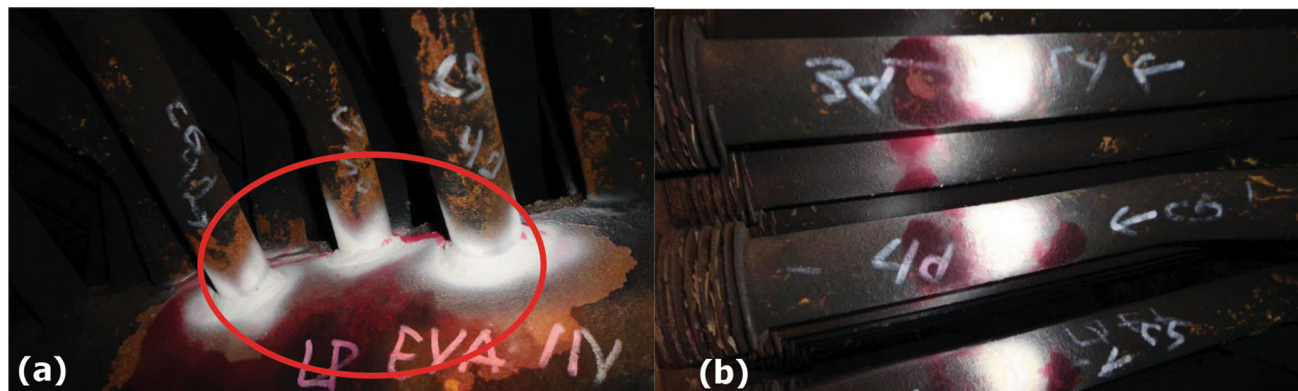


Fig. 7 NDT of the LP evaporator inlet: (a) header and (b) pipes

on the LP evaporator pipes remains permissible according to ASME B31.1 for power piping [16].

Metallographic Test

The base material’s microstructure is that of an LP evaporator pipe made of ST37.8 CL1, as shown in Fig. 8. The inspection results (Fig. 8b) align with an ASTM A178 [17] standard (Fig. 8a), as both indicate the presence of ferrite phase (indicated by a red arrow) and pearlite (indicated by a black arrow). No significant changes in the macro or microstructures were detected, and the grain shape appeared coarse.

SEM-EDS

The results of the SEM are displayed in Figs. 9 and 10 for both the inner and outer cross-sections of the LP evaporator

pipes. In addition, a description of the entire sample is provided below.

Sample 1 was a segment of the LP evaporator pipe’s eastern section, displaying general corrosion and pitting corrosion on the outer surface caused by sulfur (refer to area 3 in Fig. 9 section of the cross-section of the outer surface of the pipe). An oxide corrosion layer is also observed on the pipe’s outer surface. The sulfur content in the outer material originates from the flue gases generated during fuel combustion. The base metal’s grains reveal a composition of ferrite and pearlite with large grain sizes, a characteristic that allows the eastern pipe to endure high temperatures for maximum grain development. However, the presence of large grains implies a reduction in the pipe material’s strength. The tensile testing conducted in this area resulted in a range of 25 kg/mm². The SEM outcomes did not identify grain boundary cracks, creep, precipitates, or inclusions in the material grains.

Sample 2 represents the west-side pipe and exhibited generally acceptable grain conditions, indicating a reasonably high strength. Its tensile strength, was measured to be around 35 kg/mm². Upon examining the pipe’s outer and inner surfaces, there was evidence of pitting corrosion on the outer surface in area 4. In addition, there is a possibility of stress corrosion cracking (SCC) on both the outer surface (area 4) and inner surface (area 1). Cracks that propagated in the longitudinal direction were observed on the pipe’s inner surface. Furthermore, there was evidence of pitting corrosion and erosion in area 3 of the inner

Table 2 UT thickness measurement results

Position	Design thickness (mm)	Minimum measured thickness (mm)	Standard measured thickness (mm)
C1	2.9	2.62	1
C2		2.7	
C3		2.15	
C39		2.67	
C40		2.5	

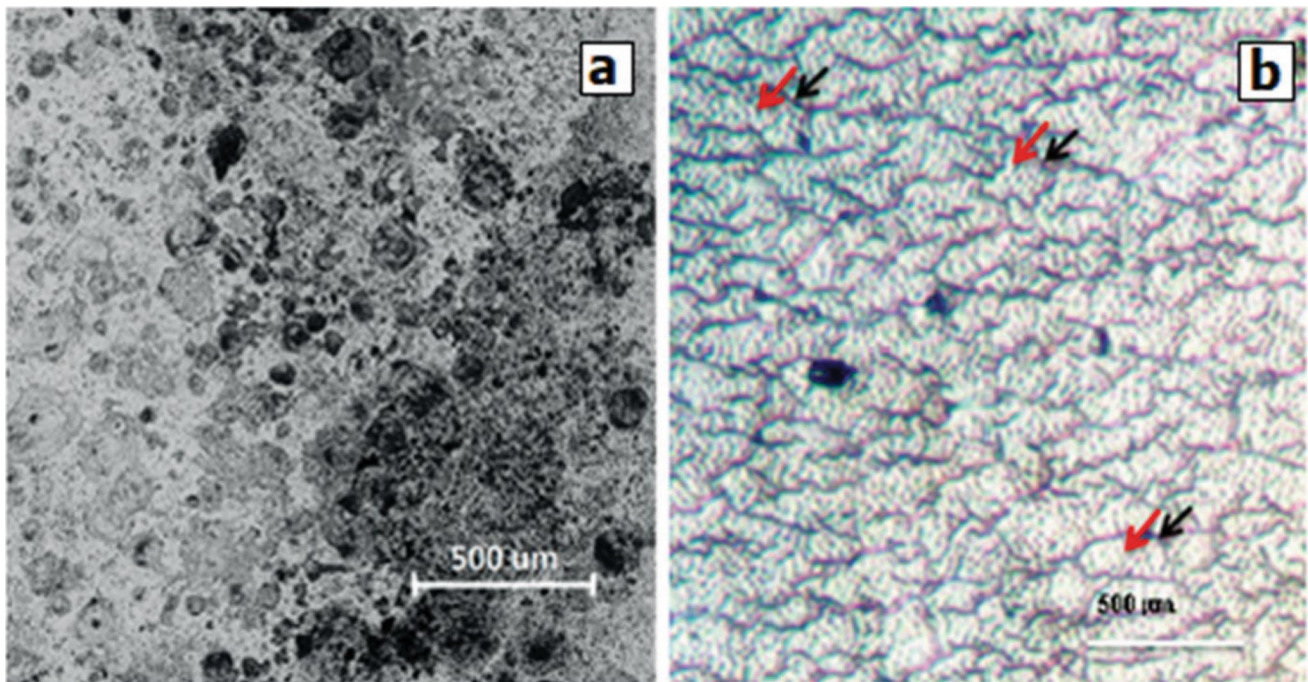


Fig. 8 Metallography result: (a) ASTM A178 and (b) inspection result with 500x

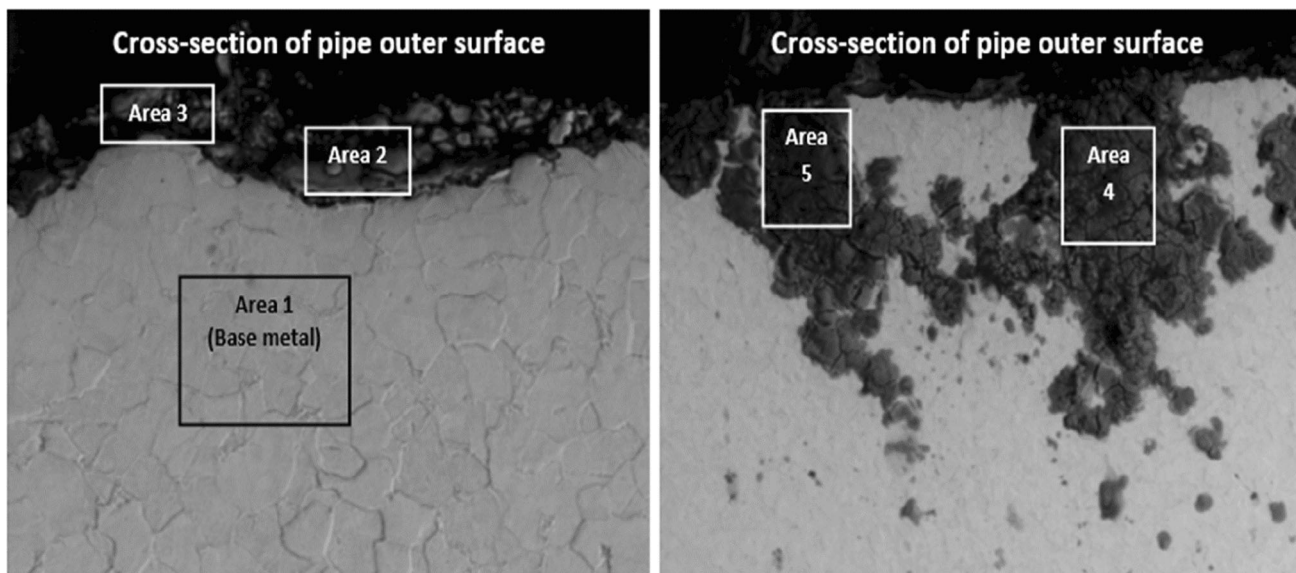


Fig. 9 SEM images: Cross-section of the pipe's outer surface (Sample 1)

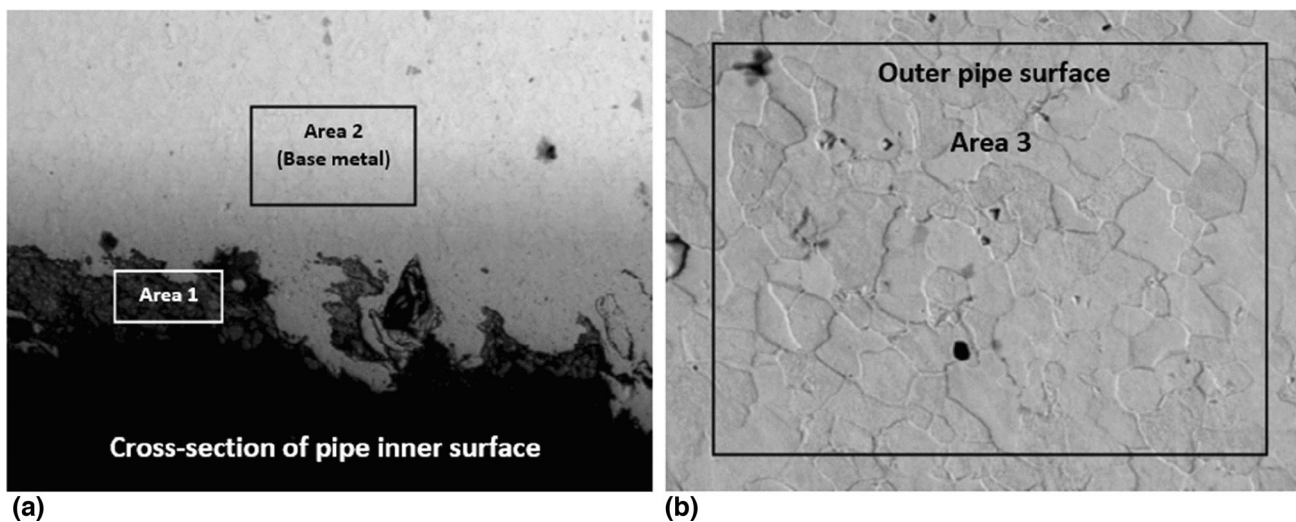


Fig. 10 SEM image of Sample 1: (a) cross-section of the pipe's inner surface and (b) outer pipe surface

surface, which allowed for the occurrence of flow-accelerated corrosion (FAC).

EDS was used to determine the chemical composition of the fracture surface. Table 3 shows that the EDS results for Sample 1 of the pipe's outer surface contained 0.23 and 0.03% Cl for areas 4 and 5, respectively (Table 4). Table 5 indicates that Cl levels of 0.11% were also found in area 4 of Sample 2 of the outer surface, which could have caused the failure of the LP evaporator pipe. However, the Cl element was not present on the pipe's inner surface in either samples 1 or 2 (Tables 4 and 6). Typically, the abundance of Cl elements in the pipe leads to corrosion and ultimately, leaks [18].

Table 3 EDS experiment result of Sample 1

Elements	Chemical compositions (% mass)				
	Area 1	Area 2	Area 3	Area 4	Area 5
C	19.10	20.24	20.06	20.77	22.97
O	...	27.37	29.33	28.62	28.15
Si	0.18	0.30	0.13	0.10	0.13
Cl	0.23	0.03
S	0.30
Ca	...	0.16	0.14
Fe	80.72	51.93	50.04	50.28	48.72

Table 4 EDS experiment result of Sample 1

Elements	Chemical composition (% mass)		
	Area 1	Area 2	Area 3
C	20.51	7.54	4.05
O	25.26
Si	0.22
Fe	52.50	92.46	95.95
Zn	1.52

Table 5 EDS experiment result of Sample 2

Elements	Chemical composition (% mass)				
	Area 1	Area 2	Area 3	Area 4	Area 5
C	15.10	18.84	29.37	27.64	14.78
O	...	35.19	12.08	30.17	...
Si	0.10	0.44	0.24	2.24	1.25
Cl	0.11	...
S	...	0.13
Ca	0.21	...
Fe	84.80	45.39	58.30	39.63	83.96

Table 6 EDS experiment result of Sample 2

Elements	Chemical composition (% mass)			
	Area 1	Area 2	Area 3	Area 4
C	48.68	16.17	16.37	4.85
O	13.22	22.58	16.63	...
Si	0.12	0.19
Ca	0.37
Ti	1.37	2.54	1.70	...
Fe	36.24	58.72	65.31	94.96

Tensile and Hardness Measurement

The tests conducted on the west-side pipe reveal a maximum tensile strength of approximately 35 kg/mm². In contrast, the eastern section of the LP Evaporator pipe demonstrates a maximum tensile strength within the range of 22 kg/mm². The material’s tensile strength for the LP Evaporator pipe design conditions is 37.8 kg/mm². The variation in tensile strength between the design conditions and the current material installation is likely due to fatigue from the cyclic loads experienced during the HRSG system’s on-and-off operation. This results in the pipe stretching and shrinking several times, leading to a reduction in strength in the area near the bend. In addition, the eastern pipeline is exposed to higher temperatures as more flue gas flows through that side, leading to faster

fatigue compared to the western pipeline. The pipe exposed to higher temperatures experiences more significant expansion, resulting in the eastern pipeline experiencing cyclic loads with larger amplitude, leading to more significant strength reduction compared to the west-side pipe.

Furthermore, the hardness test conducted on the failure zone of both the east and west sides of the LP evaporator pipes revealed an average value of around 131.3 HB and 133.5 HB, respectively. This indicates a change in hardness near the lip rupture (samples 1 and 2 in Fig. 5) compared to the area away from the lip rupture (Sample 3 in Fig. 5). Therefore, according to ASTM A178 [16] grade A for carbon-steel welded boiler tube material hardness, which has a value of 139, the significant drop in hardness around the lip rupture indicated that creep damage and material softening occurred during operation.

Thermal Analysis and Thermography

In the preceding section, various measurements were conducted to identify the reason behind the failure on the western side of the LP evaporator pipe. However, none of the measurements yielded significant results, suggesting that other factors, including thermal effects, may have contributed to the issue. Thus, this subsection will delve into the analysis of thermal failure and will utilize thermographic measurements to verify the findings of thermal fatigue calculations (Figs. 11 and 12).

Table 7 presents calculation results based on the equations presented in the preceding subsection to determine the flexibility of both sides of the LP evaporator due to excessive thermal stress. From the results, the flexibility criterion ($\frac{(D.Y)}{(L-U)^2} < 0.03$) of the eastern LP evaporator pipe is slightly higher than that specified ($\frac{(D.Y)}{(L-U)^2} = 0.04$), with a difference of 0.01, suggesting that the risk of thermal-induced failure was significant. To demonstrate this, we conducted thermographic measurements on the east and west sides of the LP evaporator pipe to determine the difference between the actual and design inlet temperatures. Figure 13 shows the results of these measurements. In the recorded image (Fig. 13a), the east side appears significantly warmer than the west-side. By translating the thermographic images into temperature values, we determined that the maximum temperature on the east side wall is about 280.3 °C (Region 3), while the maximum temperature on the west-side wall is about 90 °C (Region 2), as seen in Fig. 13b. This indicates that the outlet section is exposed to higher heat levels than the inlet section. The uneven gas flow pattern is responsible for this difference, which often leads to damage at the outlet. Region 3 on the east side of the outlet is the hottest area, with an average

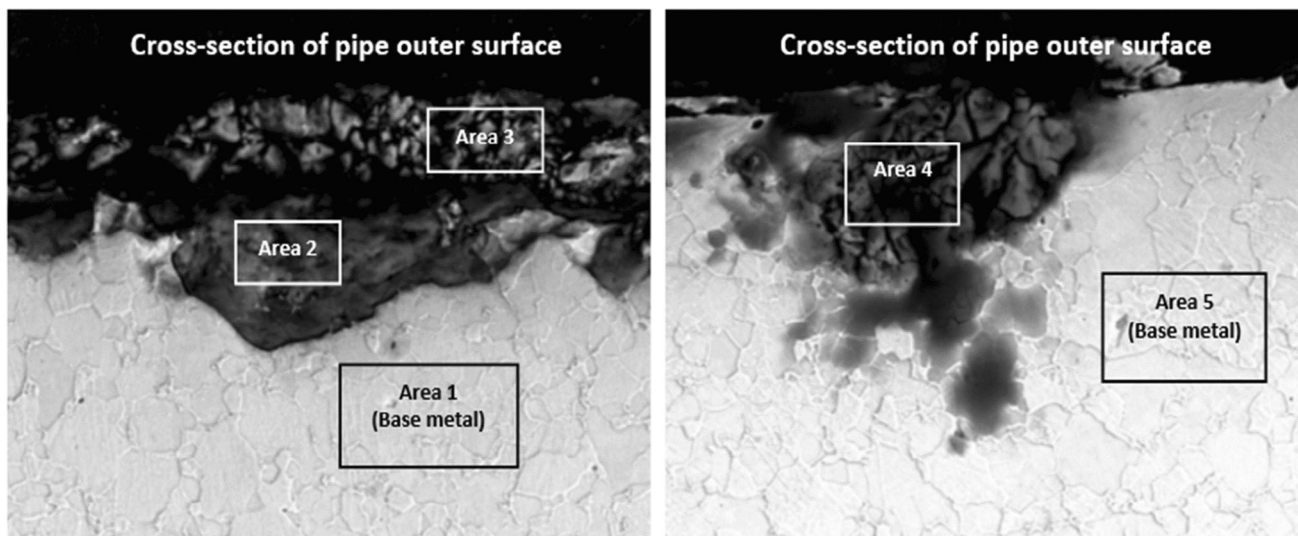


Fig. 11 SEM images of Sample 2: Cross-section of the pipe’s outer surface

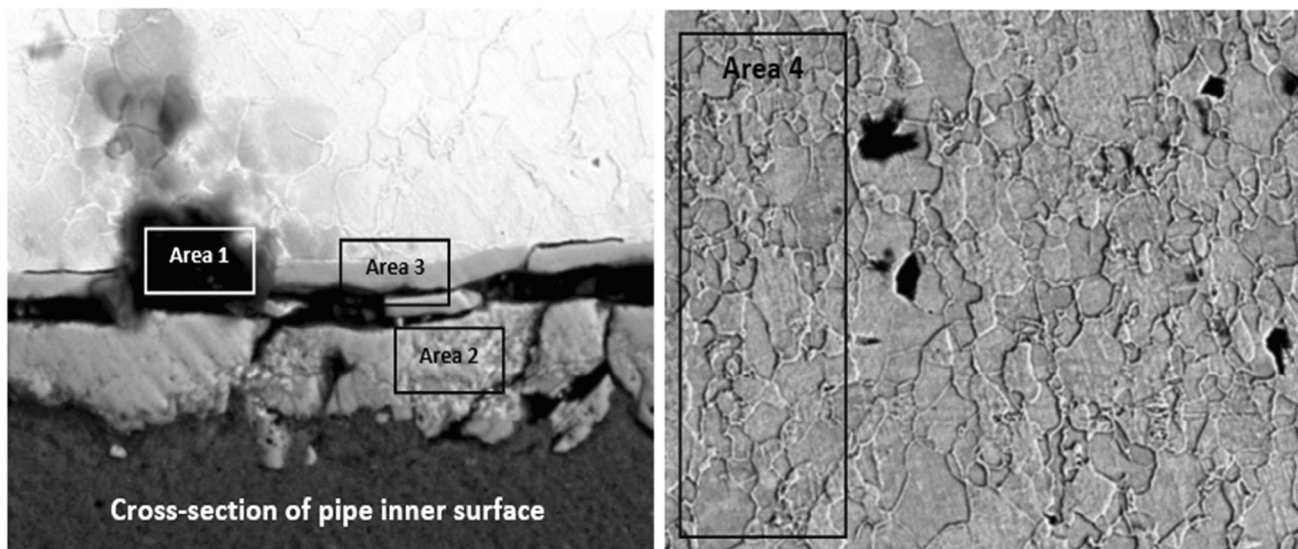


Fig. 12 SEM image of Sample 2: Cross-section of the pipe’s inner surface

Table 7 Flexibility criterion result

	East side ($T_1 = 270\text{ }^\circ\text{C}$)	West-side ($T_1 = 90\text{ }^\circ\text{C}$)
α_{-1}	$13.1 \times 10^{-6}\text{ m/m}\cdot^\circ\text{C}$	$12.1 \times 10^{-6}\text{ m/m }^\circ\text{C}$
α_{ambient}	$11.7 \times 10^{-6}\text{ m/m}\cdot^\circ\text{C}$	$11.7 \times 10^{-6}\text{ m/m }^\circ\text{C}$
y_v	0.00134 m	0.00031 m
y_h	0.0522 m	0.012 m
y_R	0.0523 m	0.012 m
$\frac{(D.Y)}{(L-U)^2}$	0.04	0.009

temperature of approximately 240 °C. This is because the weld in this region has a larger mass than the welds in other regions, such as Region 2 and Region 1, which have

average temperatures of around 218.1 and 208.6 °C, respectively. Additionally, the average temperatures of the LP evaporator on the west and east sides showed a significant difference from the design temperature, as shown in Fig. 1. The largest difference was found on the west-side, with a 100 °C variance between the actual and design temperatures. This temperature difference caused non-uniform expansion of the evaporator pipes, resulting in the east side pipe being longer than the west-side pipe and causing thermal stress in the LP evaporator pipe system (Table 8).

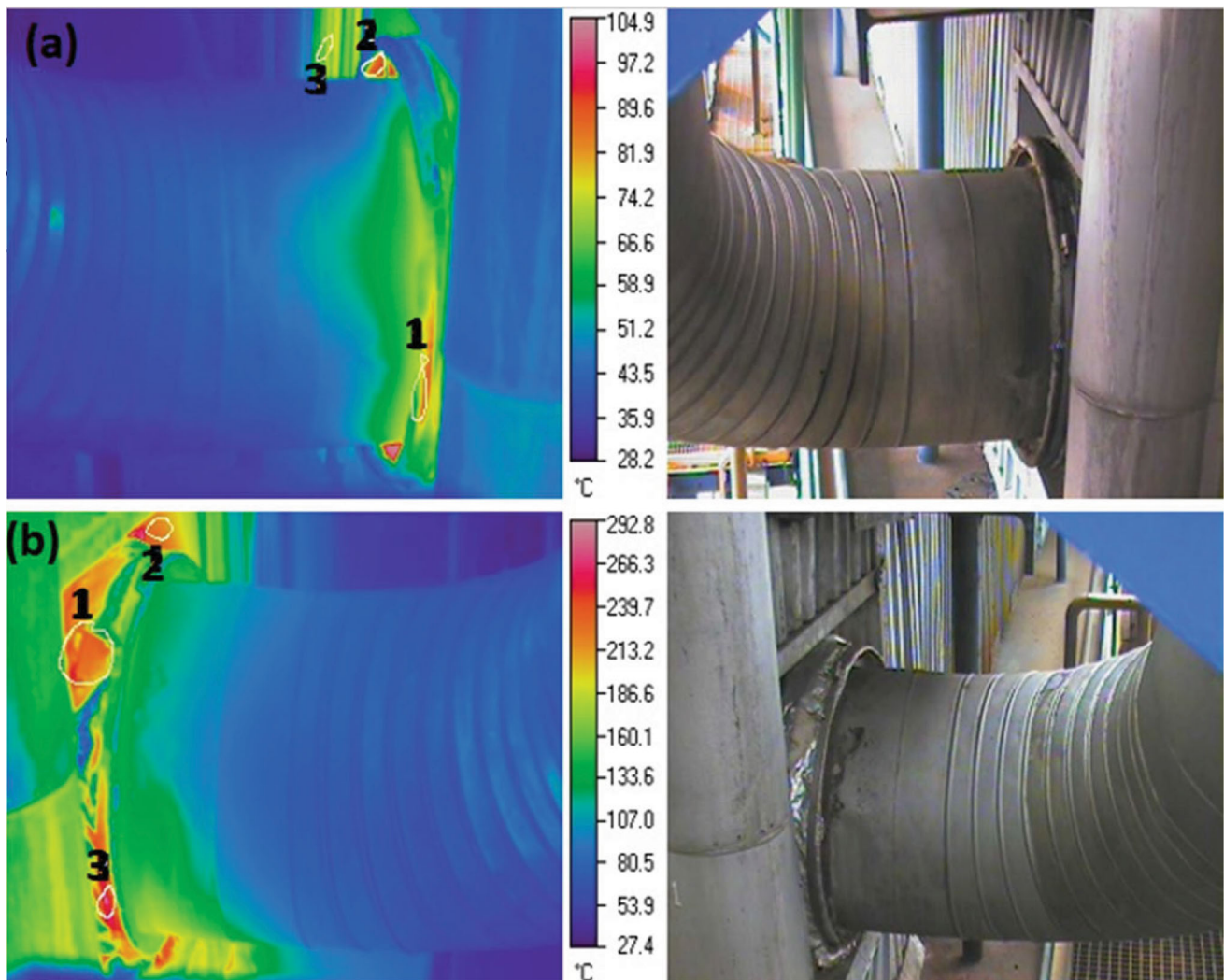


Fig. 13 Thermography result of the LP evaporator: (a) west-side and (b) east side

Table 8 The result of thermography measurement

	East side of LP evaporator			West-side of the LP evaporator		
	Region 1	Region 2	Region 3	Region 1	Region 2	Region 3
Avg pal (°C)	73.4	77.2	67.6	208.6	218.1	240.6
Min pal (°C)	56.4	43.8	60.7	122.7	204.5	163.1
Max pal (°C)	86.6	90.7	72.8	253.1	235.6	280.3

Conclusion

Based on the investigation into the failure of the LP evaporator pipes, several conclusions can be drawn as outlined below:

- Damage to the LP Evaporator pipe often occurs, particularly at the connection of the header pipe, the pipe bend, and the pipe connection. On average, LP Evaporator pipes failed 1.1 times per year, resulting in an annual failure rate.
- A partial replacement of the east side of the LP Evaporator header was necessary due to cracks in the header. The header required several welding processes during the repair.
- The thickness measurements indicate that the LP Evaporator pipe bend on the east side is thinner than the western part of the pipe. This is likely due to the higher flow rate of flue gas on the east side, causing the eastern pipe to be exposed to higher temperatures. Materials subjected to high temperatures experience a decrease in strength and hardness, making them more susceptible to erosion from the flow.

- The metallographic examination revealed that the microstructure of the west-side pipe of the LP Evaporator did not change significantly, but there was evidence of pitting corrosion in certain areas. It is typical for the microstructure on the east side to experience grain reduction or flattening. Typically, the change in microstructure occurs at the pipe's bend.
- Based on the results of the SEM and EDS analyses, it was observed that the western grains are refined, whereas the eastern parts are coarse. In terms of tensile strength, the western pipe had a strength of approximately 35 kg/mm², while the eastern pipe had a strength of about 25 kg/mm². While, both sides exhibited pitting corrosion, and only the eastern side showed signs of SCC.
- The LP Evaporator is subject to failure mechanisms resulting from thermal expansion and pitting corrosion.

Recommendation

Therefore, there are some recommendations for further action:

- Monitoring of flue gas flow in HRSG. It is advisable to install temperature gauges on the wall of the evaporator pipe at multiple locations to monitor flue gas flow in the HRSG. If the temperature readings are inconsistent, it indicates significant pipe fin deposition, resulting in blockage of gas flow in certain areas. In this case, operations must be immediately halted, and the pipe wall cleaned. The use of a thermocouple is a reliable and cost-effective alternative to a flue gas flow sensor.
- Replace the header pipe support with a support system that enables freedom of movement for the header pipe end both transversely and parallel to the pipe axis.
- Check the silencer before the HRSG for any damage that may be causing non-uniform gas flow. If repairs are needed, they should be promptly carried out.

Funding Open access funding provided by Hungarian University of Agriculture and Life Sciences.

Open Access This article is licensed under a Creative Commons Attribution 4.0 International License, which permits use, sharing, adaptation, distribution and reproduction in any medium or format, as long as you give appropriate credit to the original author(s) and the source, provide a link to the Creative Commons licence, and indicate if changes were made. The images or other third party material in this article are included in the article's Creative Commons licence, unless indicated otherwise in a credit line to the material. If material is not

included in the article's Creative Commons licence and your intended use is not permitted by statutory regulation or exceeds the permitted use, you will need to obtain permission directly from the copyright holder. To view a copy of this licence, visit <http://creativecommons.org/licenses/by/4.0/>.

References

1. A. Mokhtar, M. Bahrin, Failure analysis of high pressure high temperature super- heater outlet header tube in heat recovery steam generator. *Fail. Anal. Prev.* (2017). <https://doi.org/10.5772/intechopen.72116>
2. G. Prayogo, G. Haryadi, R. Ismail, S. Kim, Risk analysis of heat recovery steam generator with semi quantitative risk based inspection API 581. *AIP Conf. Proc.* (2016). <https://doi.org/10.1063/1.4945516>
3. F. Carazas, C. Salazar, G. Souza, Availability analysis of heat recovery steam generators used in thermal power plants. *Energy.* **36**(6), 3855–3870 (2011). <https://doi.org/10.1016/j.energy.2010.10.003>
4. T. Kim, D. Lee, S. Ro, Analysis of thermal stress evolution in the steam drum during start-up of a heat recovery steam generator. *Appl. Therm. Eng.* **20**(11), 977–992 (2000). [https://doi.org/10.1016/s1359-4311\(99\)00081-2](https://doi.org/10.1016/s1359-4311(99)00081-2)
5. X. Luo, Z. Zhang, Leakage failure analysis in a power plant boiler. *IERI Procedia.* **5**, 107–111 (2013). <https://doi.org/10.1016/j.ieri.2013.11.078>
6. M. Nurbanasari, H. Abdurrachim, M.M. Prihadi, Failure analysis of secondary superheater tube in a 600-mw coal power plant. *J. Fail. Anal. Prev.* **19**, 453–460 (2019). <https://doi.org/10.1007/s11668-019-00619-9>
7. G. Gupta, S. Chattopadhyaya, Critical failure analysis of superheater tubes of coal-based boiler. *Stroj. Vestn. J. Mech. Eng.* **63**(5), 287–299 (2017). <https://doi.org/10.5545/sv-jme.2016.4188>
8. D. Jones, Creep failures of overheated boiler, superheater and reformer tubes. *Eng. Fail. Anal.* **11**(6), 873–893 (2004). <https://doi.org/10.1016/j.engfailanal.2004.03.001>
9. A. Saha, H. Roy, Failure investigation of a secondary super heater tube in a 140 MW thermal power plant. *Case Stud. Eng. Fail. Anal.* **8**, 57–60 (2017). <https://doi.org/10.1016/j.csefa.2017.05.001>
10. A. Pramanick, G. Das, S. Das, M. Ghosh, Failure investigation of super heater tubes of coal fired power plant. *Case Stud. Eng. Fail. Anal.* **9**, 17–26 (2017). <https://doi.org/10.1016/j.csefa.2017.06.001>
11. G.A. Lamping, R.M.J. Arrowood, Manual for investigation and correction of boiler tube failures. Final report. Southwest Research Institute, San Antonio, USA (1985)
12. Z. Hu, D. He, X. Wu, Failure analysis of T12 boiler re-heater tubes during short-term service. *J. Fail. Anal. Prev.* **14**(5), 637–644 (2014). <https://doi.org/10.1007/s11668-014-9859-6>
13. S. Srikanth, B. Ravikumar, S. Das, K. Gopalakrishna, K. Nandakumar, P. Vijayan, Analysis of failures in boiler tubes due to fireside corrosion in a waste heat recovery boiler. *Eng. Fail. Anal.* **10**(1), 59–66 (2003). [https://doi.org/10.1016/s1350-6307\(02\)00030-4](https://doi.org/10.1016/s1350-6307(02)00030-4)
14. S. Chaudhuri, Some aspects of metallurgical assessment of boiler tubes—Basic principles and case studies. *Mater. Sci. Eng. A.* **432**(1–2), 90–99 (2006). <https://doi.org/10.1016/j.msea.2006.06.026>

15. R. Meena, Pipe stress analysis: piping design for loading types, retrieved from <https://www.littlepeng.com/single-post/2020/05/17/20-Piping-Design-For-Loading-Types>. Accessed 10 Aug 2023
16. ASME International. Power piping: ASME code for pressure piping B31, The American Society of Mechanical Engineers (2018)
17. ASTM International and A. Astm. 178/A 178M-Standard specification for electric-resistance-welded carbon steel and carbon-manganese steel boiler and superheater tube. ASTM International, West Conshohocken (2002)
18. P.K. Sen, H. Adeli, A new steel expansion joint for industrial plants: bubble joint. *Int. J. Press. Vessel Pip.* **83**(6), 447–463 (2006)

Publisher's Note Springer Nature remains neutral with regard to jurisdictional claims in published maps and institutional affiliations.